# Implementation of an Unsteady PSP System in the NASA Transonic Dynamics Tunnel

Daniel T. Reese,* Sarah M. Peak,† Kyle Z. Goodman,‡ and A. Neal Watkins*
*NASA Langley Research Center, Hampton, VA, 23666, USA*

**An unsteady pressure-sensitive paint (uPSP) system has been developed to provide time-resolved pressure measurements in the NASA Langley Transonic Dynamics Tunnel (TDT). Obtaining these measurements necessitated the development of environmental enclosures to protect the high-speed camera and ultraviolet lights required for uPSP from the harsh environment present during tunnel operation. Since the facility main drive was non-functioning during the testing window, performance of the uPSP system was demonstrated using an impinging jet with a passive oscillator attachment to provide unsteady flow with a known frequency independent of amplitude. Measurements were obtained for tunnel pressures ranging from 565 to 2116 psf, and model angles of attack between -4° and 4°. Results indicate that the system is capable of measuring surface pressure differentials on the order of 0.01 psi at full scale with a camera frame rate of at least 10 kHz. Spectral analysis shows that the fundamental frequency of the oscillating jet is captured by the uPSP system, as are the second and third harmonics. Dynamic mode decomposition highlights the dominant coherent spatial structures of the surface pressure, along with the associated frequency and growth rate of each mode, allowing for a de-noised reconstruction of the uPSP measurements. The experimental campaign outlined within this report also confirmed compatibility of the uPSP system with the TDT facility data acquisition system, and verified the successful integration with existing processing capabilities within the NASA advanced supercomputing environment.**

## I. Introduction

Accurate determination of spatially-continuous pressure distribution on aerodynamic surfaces is critical for the understanding of complex flow mechanisms and for comparison with computational fluid dynamics (CFD) predictions. Precise measurement is especially challenging in cases where an aerodynamic surface may experience unsteady flow, such as launch vehicles in transonic flight conditions.[1–7] Currently, ground test facilities make these measurements using conventional unsteady pressure transducers. While this approach provides accurate pressure information, these transducers are limited to providing data at discrete points. Moreover, the integration of a sufficient number of these dynamic pressure transducers into a scale model can be time and labor intensive, as well as costly. A number of these limitations can be mitigated through application of pressure sensitive paint (PSP),[8–11] a powerful optical technique that provides direct high-resolution measurements of pressure on an aerodynamic surface.

The PSP technique[12–16] makes use of the oxygen sensitivity of luminescent probe molecules suspended in gas-permeable binder materials. When a luminescent molecule absorbs a photon, it transitions to an excited singlet energy state. The molecule can then recover back to the ground state by the emission of a photon of a longer wavelength; this recovery is known as a radiative process. However, certain materials can also interact with an oxygen molecule such that the transition back to the ground state is non-radiative in a process known as collisional quenching. PSP exploits this collisional quenching to provide pressure measurements. Conventional PSP formulations typically have slow response times (on the order of hundreds of milliseconds to several seconds) relegating their use to more static flows; however, recent chemistry advances have resulted

*Research Engineer, Advanced Measurements and Data Systems Branch.
†Research Scientist, National Institute of Aerospace.
‡Research Chemist, Analytical Mechanics Associates.

in the development of formulations that can respond at frequencies up to 20 kHz.[17] Known as unsteady PSP (uPSP), this technique provides a means to non-intrusively measure time-resolved global surface pressures. The uPSP technique has previously been used to investigate rotating turbomachinery[18–22] and film-cooling effectiveness on gas turbine blades.[23–25] Recently, uPSP was expanded to investigate flexible rotor blades in both hover and forward flight conditions.[26–30] With the advent of improved lighting and camera technology, the uPSP technique is now being used more often in larger ground testing facilities, especially on launch vehicle models at transonic conditions.[31–33]

This report describes the implementation of a uPSP system in the NASA Langley Transonic Dynamics Tunnel (TDT), thus extending the application of the uPSP technique to a large-scale, transonic wind tunnel capable of varying the ambient pressure and test medium. The performance of the uPSP system is characterized using an impinging jet with a passive oscillator attachment used to provide unsteady flow with a known frequency independent of the amplitude. The following section details the experimental setup used to obtain the first uPSP measurements in the TDT. Results are presented in section III, followed by a discussion in section IV. Finally, conclusions are drawn and future work is proposed in section V.

## II. Experimental Setup

This section outlines the experimental setup used to provide the uPSP measurements discussed later in this paper. Section II.A describes the TDT facility, while section II.B provides details on the unsteady flow system and launch vehicle model that were used to confirm the proper behavior of the uPSP system. Section II.C clarifies the interplay between the various components and subsystems comprising the uPSP system that was developed for use in the TDT.

### A. TDT Facility

NASA's TDT is a closed-circuit, continuous-flow, variable-pressure wind tunnel located on Langley Air Force Base in Hampton, Virginia. The wind tunnel's 16×16 foot slotted test section (with cropped corners) and 15 foot diameter control room are contained within a 60 foot diameter outer pressure shell. Although the measurements discussed in this report were taken in air, the facility is also capable of using R-134a (1,1,1,2-tetrafluoroethane) heavy gas as a test medium to match the full-scale dynamic characteristics of a flight vehicle using a sub-scale model, while simultaneously matching the Mach number and providing a higher Reynolds number than air.[34] The total pressure of the tunnel can be selected in a continuous range from 0.01 to 1 atmosphere, with a maximum dynamic pressure of 550 psf in R-134a or 320 psf in air. At full operation, TDT's 30,000 HP main drive provides flow at any Mach number ranging continuously from 0 to 1.2, with a maximum Reynolds number of $9.6 \times 10^6$ per foot for R-134a and $3 \times 10^6$ per foot for air. Unfortunately, the main drive was inoperable during the test window, so an unsteady flow system (described in the following subsection) was utilized to create the pressure fluctuations on the model surface. The launch vehicle model (also described in the following subsection) was sting mounted for this study, allowing for attitude adjustment, though models can also be installed in the test section using various other support techniques such as multi-cable suspension, sidewall mounting, and using the floor turntable or rotor testbed.[35] The TDT boasts exceptional flow quality, as demonstrated by studies of turbulence,[36] sidewall Mach number distributions,[37] flow angularity,[38] wall boundary layer measurements,[39] and other primary flow parameters.[40] The facility data acquisition system (DAS) is capable of providing numerous measurements from a suite of instruments, including (but not limited to) strain gauges, accelerometers, position transducers, thermocouples, and both dynamic and steady pressure sensors. An air stream oscillation system is also available for gust response studies or model excitation.[41] With over 60 years of operation, the TDT is a unique wind tunnel facility that has hosted a wide range of aerodynamic testing.[42–48]

### B. Unsteady Flow System & Launch Vehicle Model

Since the TDT main drive was inoperable during the test window, an unsteady flow system was used to provide local, time-dependent surface pressure fluctuations on a generic launch vehicle model. An impinging jet was created using a leaf blower (Toro UltraPlus model 51621), which has a variable air speed up to 260 mph and was controlled remotely from the facility control room. The jet was spatially oscillated using a NASA Langley-developed sweeping jet actuator attachment that decouples the frequency from the amplitude using a main flow channel that controls the amplitude, and a small oscillator that controls the frequency

(a) (b)

**Figure 1. Experimental setup photographs. (a) Measurement side of model showing the uPSP painted portion illuminated by UV LED lighting. The unsteady flow system is visible on the left side of the image. (b) Non-measurement side of model and view of the enclosures (black rectangles) installed in the test section side wall.**

of the oscillations.[49] This unsteady flow system provided an ideal test case for the uPSP system since the frequency of oscillations was both constant and known. The unsteady flow system can be seen on the left side of Fig. 1a, which shows the location and orientation of the leaf blower (with passive oscillator attachment) relative to the model.

The model used for testing was a generic hammerhead launch vehicle with the same outer mold line as the Model 11 originally used by Coe and Nute,[50] as well as a number of other flow visualization,[51] vehicle buffet,[31] wavenumber-frequency,[52] and CFD[53] studies. The test article consists of a payload section that is 17.4 inches long with a 9.6 inch maximum diameter and a 2 inch radius leading nose, a 24.65 inch long second stage with a constant 6 inch diameter (with the exception of two flanges added to the downstream end), and an aft booster section that expands to a 12 inch maximum diameter over 17.7 inches. The model was instrumented with 56 Kulite dynamic pressure transducers and 14 static pressure taps. Though not used for this experimental campaign, the model also contained four tri-axial accelerometers, three type-J thermocouples, and a four-component balance. The model region of interest (where uPSP measurements were obtained in this study) is visible in Fig. 1a as the bright pink region extending from the payload section to about halfway down the second stage. Figure 1b shows the opposing side of the model, with the high-speed camera and lights inside the uPSP system enclosures in the background (black rectangles mounted in the test section side wall).

## C. uPSP System

In addition to the unsteady paint formulation applied to the test article, the uPSP system developed to provide time-resolved pressure measurements in the TDT consisted of three integrated subsystems: the enclosures, the control system, and the facility interface. This section provides information detailing each subsystem as well as the connectivity and interplay between them.

### *1. Enclosures*

The "enclosures" are a collection of aluminum environmental housings located in the wind tunnel plenum that are used to protect the high-speed camera and lights from the harsh environment present during tunnel operation (such as low pressures, high temperatures, significant turbulent flow, and atomized oil in the test medium). A total of four enclosures were used during the experimental campaign detailed in this report; each maintained an interior pressure of 1 atm as the tunnel pressure was reduced, provided a constant supply of cool air to help dissipate the heat generated by the equipment contained within, and allowed for the remote control of all internal components from the control room. As shown in Fig. 2a, each housing unit is a modular design comprised of an optical panel, front section, back face, and if needed, extension sections.

The optical panel replaces a TDT test section side wall panel and, depending on the configuration used, contains five or six circular windows for optical access to the test section from the plenum. The front section mounts directly to the optical panel and contains a variety of ports for passing through BNC signals, ethernet cabling, electrical power, cooling air supply, and additional wires, pneumatics, optics, or other equipment

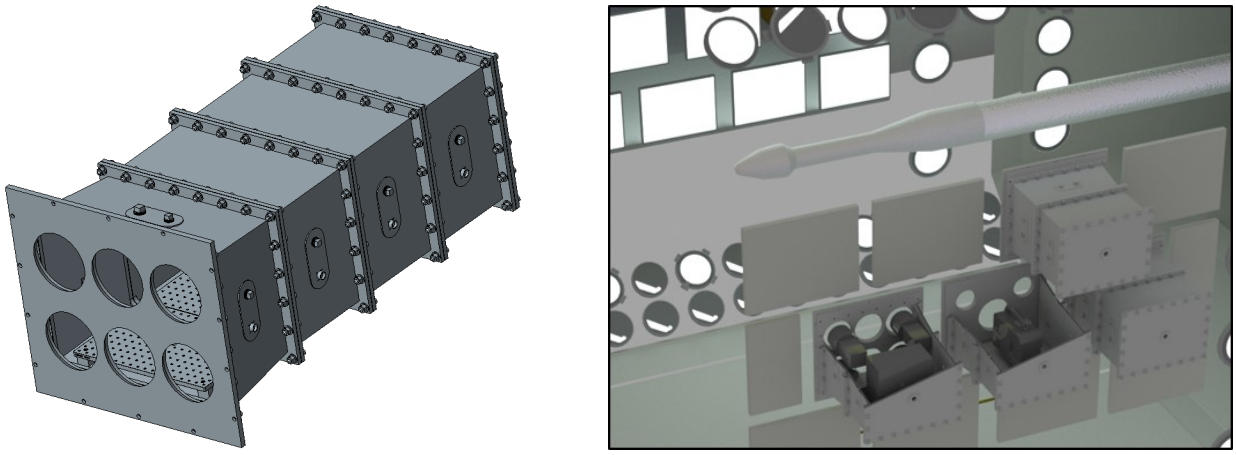

(a) (b)

**Figure 2. Environmental enclosures used to protect the high-speed camera and lights. (a) Schematic of an enclosure with four sections (only two sections were used during testing). (b) Diagram of the experimental setup showing the location of the enclosures relative to the test article.**

of interest. The interior base of the front section also allows for the attachment of a standard optical breadboard to allow for the mounting (and easy replacement) of various equipment configurations. Each extension section is optional, but provides greater interior volume and contains mounting for a breadboard base, additional wire feedthroughs, and two 3/4" holes that were used to introduce temperature and pressure sensors. Finally, the back face serves to create a pressure seal and contains a singular feedthrough for venting the cooling air supplied to the enclosure.

A schematic showing the experimental setup, including the location of the enclosures in the test section sidewall relative to the model, is provided in Fig. 2b. Three enclosures were used for lighting – each housing two dual power supply units and three or four light emitting diode (LED) heads – allowing for illumination of the model with a total of 11 UV lights. The lighting units used were the four inch, air-cooled LEDs from Innovative Scientific Solutions, Inc. (model LM4X-400), which have a peak wavelength near 400 nm with a full width at half maximum (FWHM) of approximately 17 nm. A single enclosure housed the high-speed camera that was used to collect and record the uPSP emission (Photron SA-Z with a Nikon Nikkor 85 mm $f/1.8$ lens and 650 nm bandpass filter with a 40 nm bandwidth). All enclosures were operated remotely from the control room by the control system described in the following subsection, and provided the interior pressure and temperature to the DAS for display and monitoring using the facility interface as outlined in section II.C.3.

### *2. Control System*

On the opposite side of the test section to the enclosures, the uPSP control system was located within the facility control room and consisted of a pulse generator, oscilloscope, computer, and data storage drives. The pulse generator (Berkeley Nucleonics model 575) was triggered by the facility interface during tunnel data acquisition and sent a series of pulses to the enclosure subsystem in order to control the camera and lights. These signals were monitored on an oscilloscope. In addition, data acquisition signals from the facility and output pulses from the camera (indicating active exposure and/or recording) were also monitored. Communication with the high-speed camera, including live viewing and playback of captured footage, was carried out using the Photron FastCam Viewer software (version 3.6.8.1) on the control computer, which also served as the interface for writing data to storage drives. The control system was linked to the enclosure subsystem through several BNC connections and two ethernet cables, while connection to the facility interface was provided through a single BNC connection.

### *3. Facility Interface*

The facility interface allowed for integration of the previous two subsystems with the TDT DAS.[54,55] Connection of the DAS to the enclosure subsystem enabled real-time display of the pressure and temperature

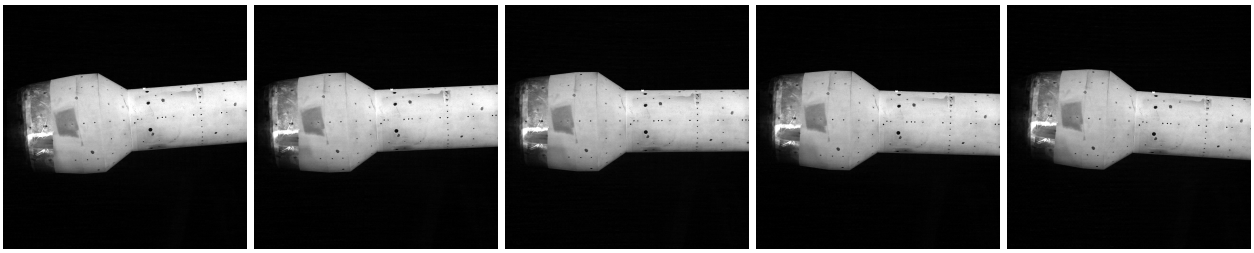

(a) (b) (c) (d) (e)

**Figure 3. Representative images of the model at various AOA as captured by the high-speed camera used for uPSP. (a)** $AOA = -4°$, **(b)** $AOA = -2°$, **(c)** $AOA = 0°$, **(d)** $AOA = 2°$, **(e)** $AOA = 4°$.

inside the enclosures from the control room, and also allowed for synchronization of uPSP measurements with dynamic Kulite sensor data by incorporating a TTL signal sent from the high-speed camera during recording. Connecting the facility DAS to the uPSP control system provided the ability to utilize a signal sent at the beginning of wind tunnel data recording to automatically turn on the UV lights, begin camera recording, and then turn off the lights after recording had completed. This way, when a uPSP dataset was desired, a single "run" button on the control system computer could be pressed which armed the uPSP system to automatically acquire data whenever the next facility datapoint was initiated. If the "run" button was not pressed, the uPSP system simply ignored the signal from the facility DAS and did not provide measurements for that datapoint.

## III. Results

The experimental setup described in the previous section allowed for the collection of uPSP data as detailed in the following subsection. A brief overview of the procedure used to convert raw intensity data to pressures (and map results to the grid) is then provided in section III.B. Processed uPSP results are post-processed to show pressure time histories and power spectral densities as discussed in sections III.C and III.D, respectively, where a direct comparison with unsteady pressure measurements from Kulite sensors is also made. Section III.E contains results from applying dynamic mode decomposition to uPSP measurements.

### A. Data Collection

Unsteady pressure sensors (hereafter referred to as Kulites) acquired data at discrete locations at 10 kHz for all conditions, while the uPSP provided global surface pressures over the entire region of interest at both 5 kHz and 10 kHz under atmospheric pressure (2116 psf) and low pressure (565 psf) conditions in air. The faster framerate allowed full-frame imaging for 4.3 seconds, while the slower framerate extended the measurement time to 8.6 seconds; the facility DAS always recorded Kulite data for 10 seconds, ensuring that the entirety of the pressure time history recorded by uPSP was captured by the DAS. For each framerate and pressure, data were collected at five angles of attack (AOAs) ranging from $-4°$ to $4°$ in $2°$ increments. Representative images showing the model at each AOA as captured by the high-speed camera are shown in Fig. 3. For each condition where uPSP data was desired, the facility would start data acquisition which automatically caused the uPSP system to begin capturing data. Once triggered, the uPSP camera would return a signal to the facility DAS indicating that recording was underway so that pressures recorded by the dynamic pressure transducers could be directly compared with measurements made by the uPSP system. Although the surface pressure fluctuations caused by the unsteady flow system were only imaged at two pressures, uPSP intensities were captured from 680 psf to 2116 psf at roughly 200 psf increments to better understand the paint emission as a function of tunnel pressure. Results of this pressure study are summarized in Fig. 4, which shows the expected decay in signal intensity as pressure is increased, owing to the larger amount of oxygen causing greater quenching at higher pressures.

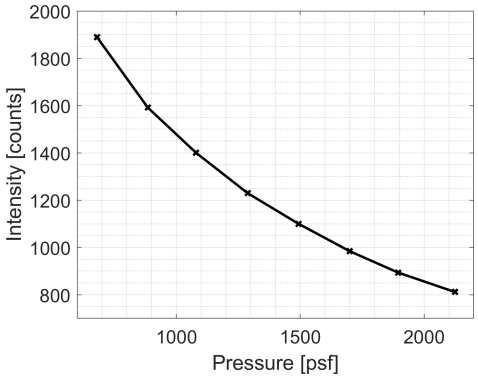


**Figure 4. uPSP signal intensity as a function of tunnel pressure showing the expected decay in signal intensity resulting from greater $O_2$ quenching at higher pressures.**

### B. uPSP Processing

Raw uPSP images captured during testing were processed using the Pleiades supercomputer[56,57] to provide surface pressures utilizing software developed and currently used by researchers at NASA Ames.[32,33,58] Data processing is broken into three phases: image preparation, intensity mapping, and conversion to pressure. In the first step, a high-accuracy calibration solution capturing the relative orientation of the camera to the test article is established for the first frame of data, and regions of "bad" uPSP data (e.g. regions containing registration targets or other small unpainted portions of the model) are patched over by interpolating camera pixel data. Any uPSP data at an oblique angle greater than 75° between the model surface normal and the camera are also removed from calculation during this step. The second phase of processing involved accounting for small model motion between frames by warping all subsequent frames to align with the first, then projecting each image onto the model grid. The final step of the uPSP processing pipeline is converting the intensity value at each grid node to pressure by calculating intensity fluctuations for each frame relative to the average of all frames[31] such that,

$$P = (I_{ref}/I - 1) * Gain. \tag{1}$$

The value for $Gain$ in Eq. (1) is calculated at each grid node using,

$$Gain = a + bT + cT^2 + (d + eT + fT^2) * P_{ss}, \tag{2}$$

where the coefficients $a - f$ are obtained through paint calibration, $P_{ss}$ is the steady-state pressure, and T is the surface temperature. The surface temperature is estimated to be the equilibrium temperature given by,

$$T = r(T_0 - T_\infty) + T_\infty, \tag{3}$$

where $T_0$ is the stagnation temperature, $T_\infty$ is the freestream temperature, and $r = 0.896$ is the turbulent boundary-layer recovery factor given by Schlichting.[59] The final output provided by the uPSP processing work flow is a time series of pressures at each model grid node visible to the camera. These results are explored further in the following three subsections.

### C. Pressure Time Histories

Representative uPSP output for the $AOA = -2°$, $P = 2116$ psf, and $framerate = 5$ kHz case is shown mapped to the grid in Fig. 5a at six distinct times in the cycle of the oscillating jet. To help reduce measurement noise and better demonstrate the effect of the unsteady flow system on model surface pressure, results have been filtered using a 15 ms moving average in time, and a $4 \times 4$ pixel 2D median filter in space. This time series of images highlights the development of a low pressure region near the shoulder of the payload section at $t = 457$ ms, which is shown to begin dissipating and moving towards the second stage of the model by $t = 463$ ms. This dissipation and downstream convection continues over the following two images (at $t = 469$ & 475 ms), during which time the development of a high pressure region emerges on the payload section. This high pressure region also dissipates and moves down the length of the model

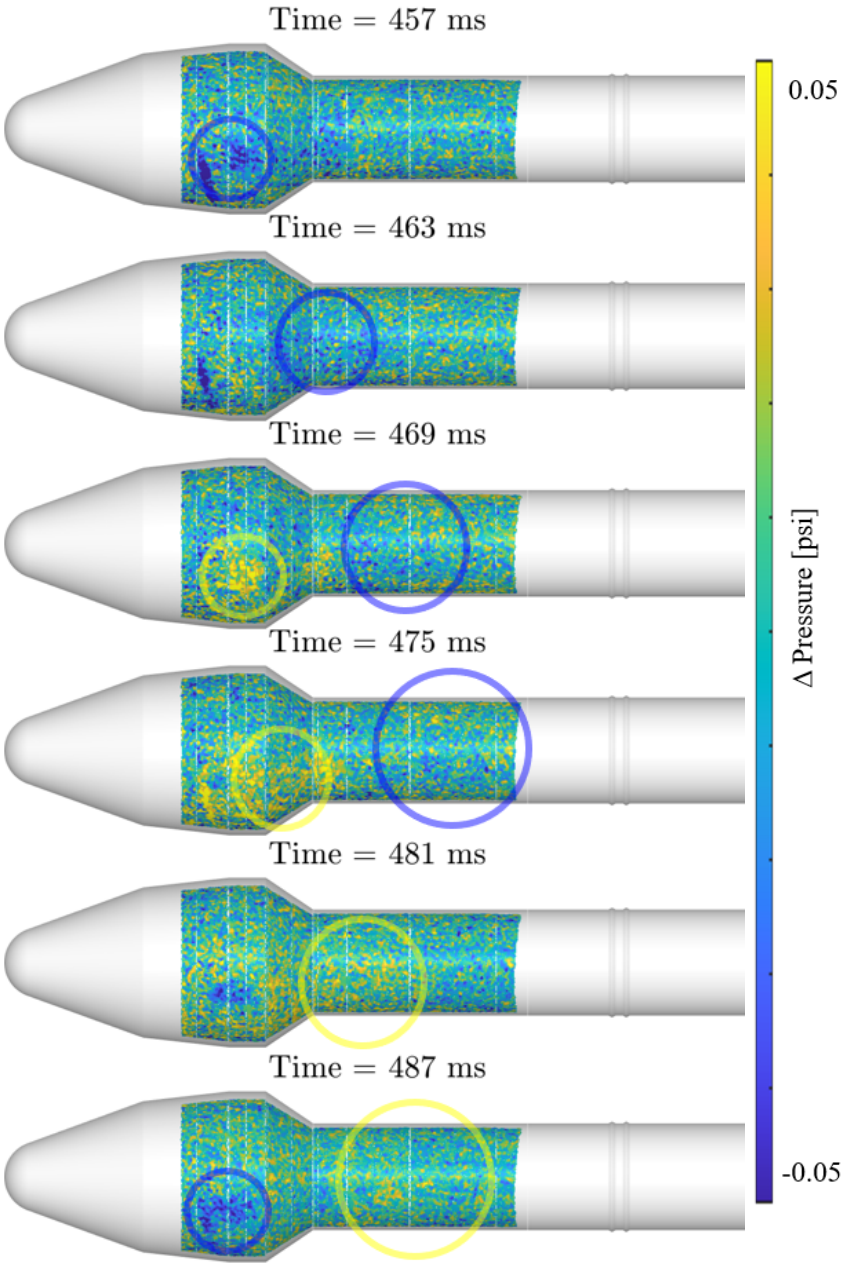


**Figure 5. uPSP results mapped to the grid. (a) Time-series of images showing the spatiotemporal effect of the oscillating jet on the model surface pressure. (b) RMS values for the entire time-series of uPSP measurements.**

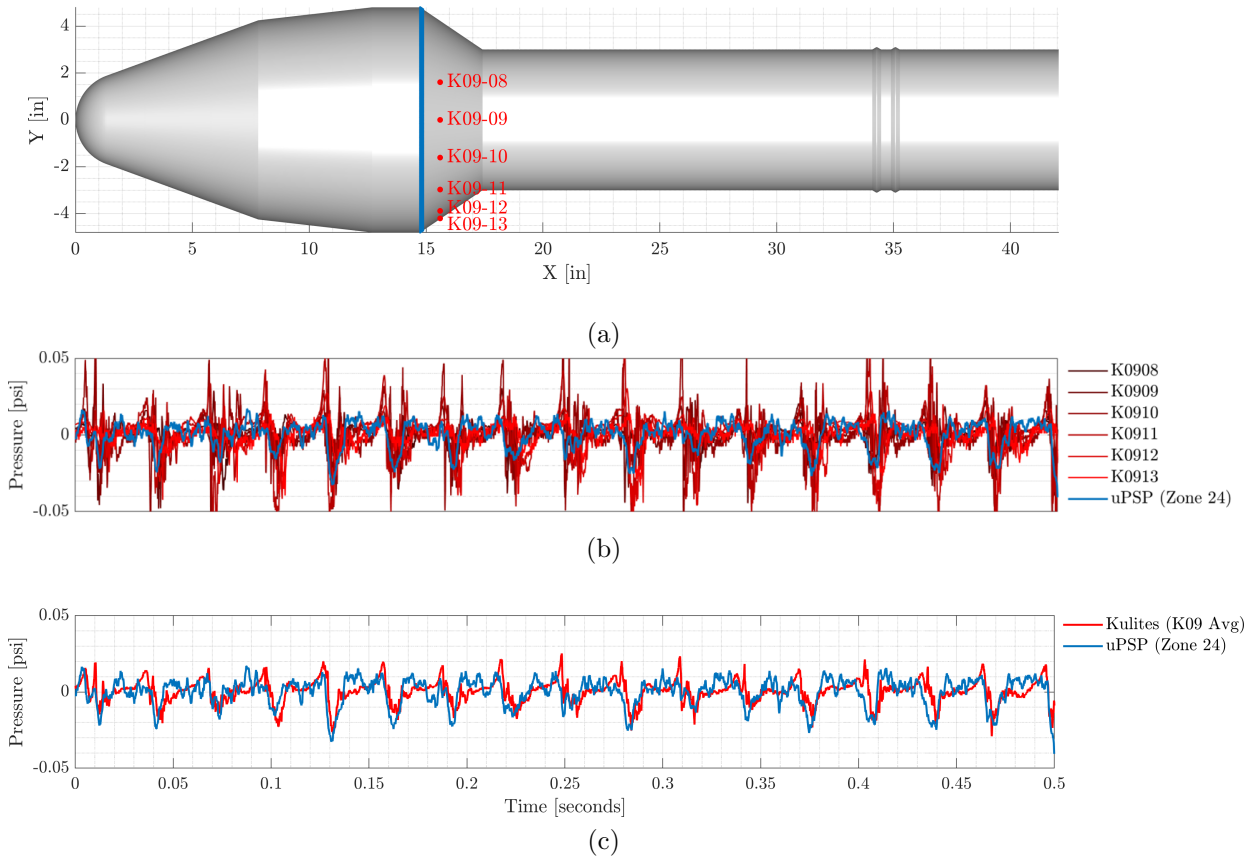


**Figure 6. Comparison of pressure time history measurements from uPSP and unsteady pressure sensors. (a) Location of the Kulites (red, labeled) and Zone 24 (blue) used for comparison. (b) Average pressure for Zone 24 plotted with pressure traces from individual Kulites. (c) Average Zone 24 pressure time history compared against average K09 sensor measurements.**

as time progresses, and by the final two frames in Fig. 5a, a low pressure region re-emerges as the cycle continues. The root mean square (RMS) of all surface pressure measurements is shown in Fig. 5b, and provides further insight into the uPSP measurements that were obtained. Figure 5b displays small sections of orange scattered throughout the measurement region, telltale signs of the patched areas where the RMS value is exceptionally low. Comparison with Fig. 3 confirms that the low-RMS patches correspond to the locations of registration targets on the model. Another notable feature evident in this figure is the nearly-rectangular region of higher RMS near the model centerline towards the most upstream location measured on the payload section. This region is the result of existing damage to the base layer of the PSP from model handling, and is likely due to wear from a support strap. Finally, Fig. 5b shows the average pressure RMS to be notably higher along the bottom half of the model, which is to be expected given the sub-centerline positioning of the leaf blower. Additionally, more light was provided from above the centerline than below, leading to a higher signal-to-noise ratio (SNR) on the top half of the model.

Since the facility DAS received a signal from the camera while recording was in progress, pressure time histories measured by the uPSP system were able to be matched directly against those obtained simultaneously by the Kulite dynamic pressure sensors. This comparison is provided in Fig. 6, where measurements from a line of Kulites located just downstream of the payload shoulder are compared against the average pressure for "Zone 24" of the model, a thin region comprising the portion of the payload section with the maximum diameter. Figure 6a shows the location for each of the six pressure sensors as indicated by red dots and labeled with the corresponding Kulite names, while Zone 24 is marked by a blue line just upstream of the Kulites. Pressure time histories for each Kulite are plotted with the average pressure of Zone 24 in Fig. 6b, which shows that all signals detect evidence of a cyclic pressure trace. Close inspection of Fig. 6b also indicates that the outermost Kulites (K09-08 & K09-13) show smaller-amplitude pressure differentials than those from Zone 24 and the "inner" Kulites, resulting from each pressure sensor's location relative to

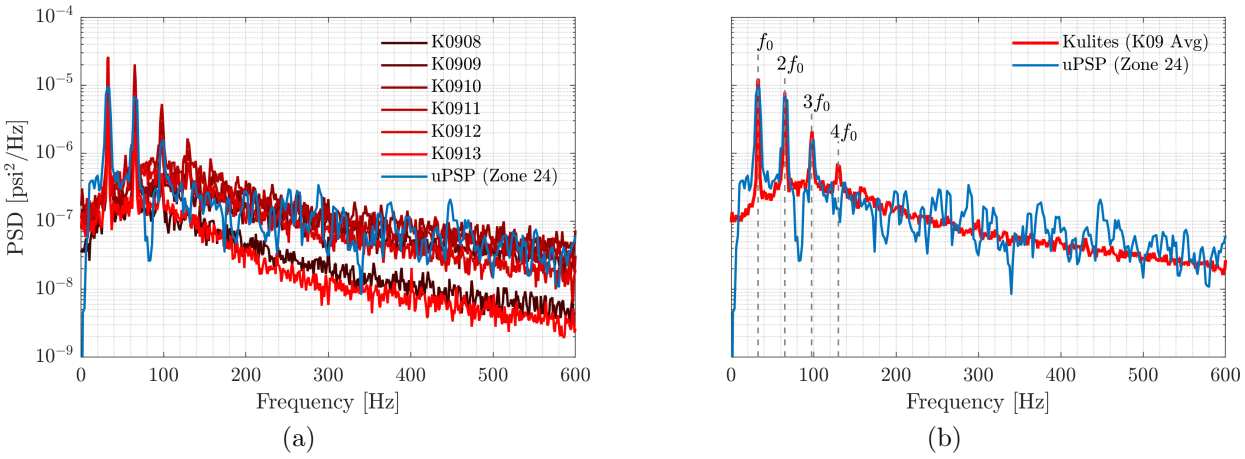


**Figure 7. Spectral comparison between uPSP and dynamic pressure sensor measurements. (a) PSD for Zone 24 compared against results from individual Kulites. (b) PSD for Zone 24 compared against the average of all K09 Kulites, showing the fundamental frequency of the oscillating jet ($f_0$) as well as the second, third, and fourth harmonics.**

the oscillating jet. A more suitable comparison between the dynamic pressure sensor measurements and uPSP results can be obtained by taking the average of all K09 Kulites; this comparison is displayed in Fig. 6c which shows similar phase and amplitude for the pressure oscillations as measured by the two methods, and indicates that one full cycle is approximately 30 ms long. This cycle period corroborates the observation from Fig. 5a where the formation, dispersion, and re-emergence of the low pressure region on the payload section takes place from roughly 457 to 487 ms. This estimate for the jet oscillation period is refined in the following subsection by making a spectral comparison of the pressure time histories, which also further confirms the spatial dependance of pressure fluctuation amplitude resulting from the influence of the jet location on the model surface.

### D. Spectral Comparison

Power spectral density (PSD) analysis of the pressure time histories provides insight into the power present in the signal as a function of frequency and is a common data product reported in uPSP studies.[31,32,52] A spectral comparison between the Kulite data and uPSP measurements covered in the previous subsection is reported in Fig. 7. Figure 7a shows the PSD for Zone 24 plotted against individual K09 Kulites and, compared to Fig. 6b, more clearly displays the difference in pressure fluctuations measured by each Kulite. More specifically, the "outer" Kulites (K09-08 & K09-13) show a significantly lower PSD value across all frequencies than the "inner" Kulites and Zone 24 as a result of their proximity to the location of jet impingement on the model surface. Plotting the PSD of the uPSP measurement against the average PSD of all K09 Kulites (shown in Fig. 7b) clearly indicates that the two methods provide similar values for the PSD across all frequencies, though the dynamic pressure transducer noise is significantly lower than that of the uPSP. This noise difference is expected to be a result of averaging pressure values over a relatively large area when compared against the local values returned by the Kulites, and can likely be mitigated by only considering uPSP measurements directly surrounding any given Kulite sensor; this topic is to be investigated further in future work. The two spectra also show the detection of the fundamental frequency of the oscillating jet ($f_0 = 32.5$ Hz) more precisely than the pressure time histories reported in Figs. 5a and 6c. Additionally, both PSDs show the detection of the second and third harmonics ($2f_0$ & $3f_0$). The average Kulite PSD also shows the ability to detect the fourth harmonic ($4f_0$), while this harmonic is indistinguishable from noise in the uPSP measurements.

### E. Dynamic Mode Decomposition

Dynamic mode decomposition (DMD)[60] is an algorithm that can be used to extract the dynamical behavior for the leading spatial modes of the evolving pressure field on the model surface. Recently, it has been applied to uPSP data.[61–63] Output of the uPSP processing software described in section III.B is ideal

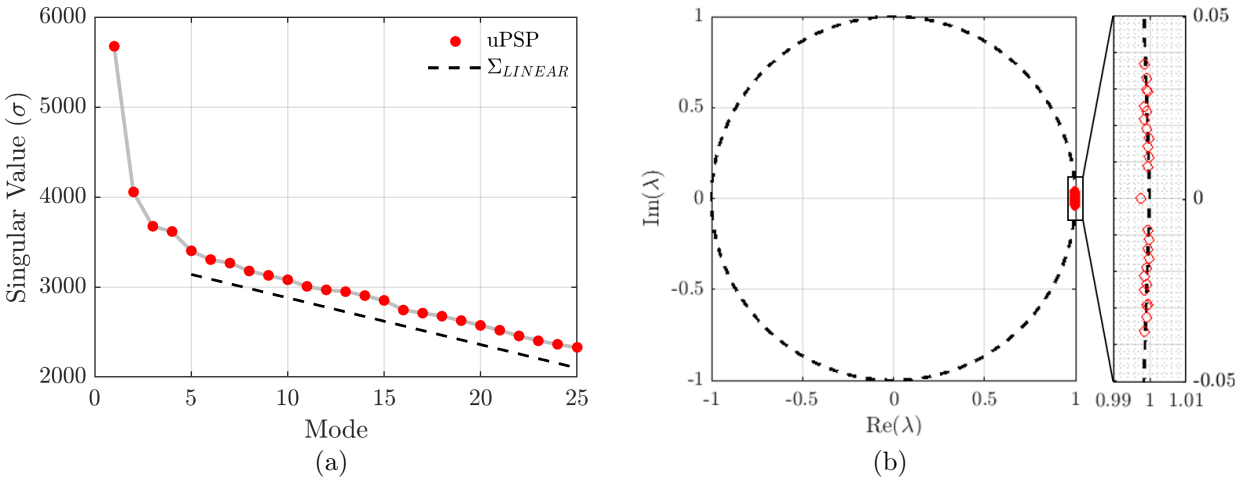


**Figure 8. DMD results from uPSP measurements. (a) Scree plot of the singular values ($\sigma_i$) corresponding to each of the 25 leading modes considered in the analysis. (b) Eigenvalue distribution showing the 25 leading eigenvalues ($\lambda_i$) of $A$ plotted in the complex plane; their proximity to the unit circle indicates stable oscillatory behavior of the associated eigen-pressure modes.**

for DMD analysis since results are comprised of a time series of high-dimensional data. Processed uPSP measurements come in the form $\hat{X} \in \mathbb{R}^{M \times N}$, where the time series of pressures is comprized of a total of $N$ frames at each of $M$ model grid nodes. In other words, the data output from the uPSP processing software is a matrix whose columns are the pressure measurements at each time,

$$\hat{X} = \{x_1, x_2, ..., x_N\}, \tag{4}$$

where $x_i \in \mathbb{R}^M$ is the $i$-th frame of the pressure field. By splitting the time series of pressure measurements into two matrices $X = \{x_1, x_2, ..., x_{N-1}\}$ and $X' = \{x_2, x_3, ..., x_N\}$, DMD seeks a best fit linear operator $A$ that advances $X$ into $X'$,

$$X' \approx AX. \tag{5}$$

Performing a singular value decomposition (SVD) of $X$,

$$X = U\Sigma V^* \rightarrow X' = AU\Sigma V^*, \tag{6}$$

where columns of $U$ are the dominant coherent structures organized from most to least important in terms of capturing the variance of $X$, $\Sigma$ is an ordered diagonal matrix of singular values, and $V^*$ contains temporal information corresponding to the modes in $U$. Projecting $A$ onto the dominant singular vectors,

$$U^*X'V\Sigma^{-1} = U^*AU \equiv \tilde{A}, \tag{7}$$

yields the reduced matrix $\tilde{A}$, which is a linear best fit dynamical system describing how the dominant pressure modes evolve in time. If the system of interest has low dimensional behavior, $\tilde{A}$ can be further reduced by considering only the first $r$ columns of $U$ in the projection shown in Eq. 7. A scree plot, shown in Fig. 8a, can be used to determine if the system has low dimensional behavior and help choose an appropriate value for the cutoff mode $r$. By plotting $\sigma_i$ (entries along the diagonal of $\Sigma$) as a function of mode, the monotonic decrease of the graph is clear and the emergence of an "elbow" where the singular values level off should become evident.[64] Though a somewhat subjective criterion for determining mode cutoff, based on the elbow in Fig. 8a (right before the linear region highlighted by the dashed line), an argument can be made that only the first four most dominant modes need to be retained in this case. Additional evidence supporting a choice of $r = 4$ is provided later in this section; however, a value of $r = 25$ was used for the work carried out in this report to ensure that contributions from higher modes were captured.

Once the number of dominant modes needed for analysis has been determined, the next step in DMD involves computing the eigendecomposition of $\tilde{A}$,

$$\tilde{A}W = W\Lambda, \tag{8}$$

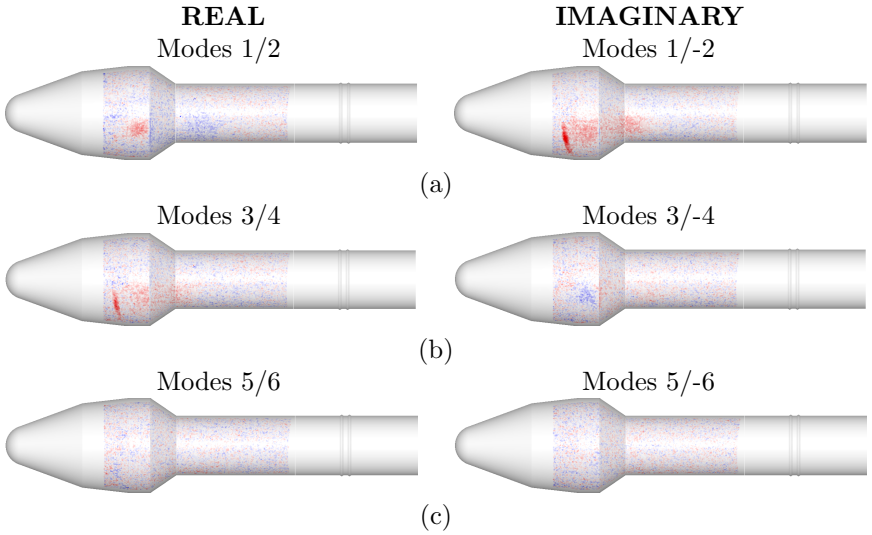


**Figure 9. Leading eigen pressure distributions showing the real and imaginary parts comprising the dominant spatial coherent structures of the uPSP data for the (a) first, (b) second, and (c) third mode pairs.**

where $W$ and $\Lambda$ are the eigenvectors and eigenvalues of $\tilde{A}$, respectively. Since $A$ has the same leading eigenvalues as $\tilde{A}$, insight into the temporal characteristics of our system can be gained from plotting $\lambda_i$ (entries along the diagonal of $\Lambda$) in the complex plane. Eigenvalues falling within the unit circle represent decaying modes, while $\lambda_i$ with a radius greater than one are associated with modes that grow in time. The complex eigenvalue distribution in the phase domain (Fig. 8b) shows that all eigenvalues lie nearly entirely on the unit circle, indicating that the dominant modes are oscillatory; this is expected given the nature of the fluidic oscillator used in the unsteady flow system driving the pressure fluctuations measured by the uPSP system. Note also that the 25 eigenvalues considered in this study are comprised of 12 complex conjugate pairs and a single real value. Additional information such as the mode frequency and growth rate can be obtained from the angle and distance to the origin of each $\lambda_i$.

With an understanding of the temporal characteristics given by the leading eigenvalues of $A$, only the corresponding eigenvectors remain to be determined. The leading eigenvectors of $A$ can be computed using the formulation from Tu et al.,[65]

$$\Phi = X'V\Sigma^{-1}W. \tag{9}$$

DMD eigenvectors (columns of $\Phi$) relate to the spatial characteristics of the system and, like the associated eigenvalues, come in complex conjugate pairs. While typically the first mode would contain the average pressure distribution and pairs would begin with modes 2 and 3, in this case data were processed relative to the steady state value, so pairing begins immediately with modes 1 and 2. The real and imaginary "eigen pressure distributions" shown in Fig. 9 highlight the dominant spatial coherent structures involved in the modal dynamics for the first three mode pairs. Figure 9a shows that for the arbitrary time considered, the first mode set consists of a real coherent structure associated with the downstream impingement point of the sweeping jet, while the imaginary mode pair is associated with the surrounding region and the upstream impingement point. The opposite is true for the second eigen pressure distribution pair shown in Fig. 9b. For both real and imaginary eigenvectors, no large coherent structures are visible in the third mode set, Fig. 9c, providing further evidence (in addition to the scree plot elbow shown in Fig. 8a) that as few as the first four dominant modes may be used to describe the dynamics of this system.

While we have thus far viewed the temporal and spatial modes of the DMD separately, each eigenvector is dynamic and coupled to a specific frequency given by the eigenvalue of that mode. This spatiotemporal coupling means that the leading dynamical behavior of the original uPSP data $\hat{X}$ can be reconstructed using only the leading $r$ dominant modes by considering both $\Phi$ and $\Lambda$ together,

$$\hat{Y}(t) = \Phi\Lambda^t z_0, \tag{10}$$

where $\hat{Y}$ is the reconstruction, $t$ is a time index, and $z_0$ is a set of coefficients determined by initial conditions. Note that Eq. 10 allows for future time predictions to be made — though caution should be used when

projecting solutions "too far" into the future. $\hat{Y}$ will more accurately represent the original uPSP measurements as additional modes are considered in the reconstruction; however, unwanted noise can be reduced by omitting certain modes. These "filtered" DMD results (where modes higher than 25 are excluded from the reconstruction) are shown in Fig. 10. When compared against the time series of spatiotemporally-averaged uPSP measurements in Fig. 5a, the reconstruction more clearly shows the influence of the unsteady flow system on the model surface pressure.

## IV. Discussion

The experimental campaign detailed in this report served to demonstrate the performance of a newly-implemented uPSP system in the TDT. Upon return to service of the facility main drive, this system will be used to make time-resolved pressure measurements on the surface of flight and launch vehicle models at conditions matching the full-scale aerodynamic characteristics. Despite the lack of full-operability of the wind tunnel, results presented in the previous section prove the success of the design, fabrication, installation, and functionality of the environmental enclosures (as well as the UV lights and high-speed camera contained within), in addition to the successful integration of the uPSP control system and TDT facility interface. Raw intensity movies acquired during this study were used to test processing capabilities on the Pleiades supercomputer, yielding the unsteady pressure measurements presented in this work. The development and maturation of data post-processing pipelines were also permitted by the efforts outlined in this paper. Ultimately, the uPSP system described herein is expected to provide dynamic pressure measurements at transonic conditions, which will allow for comparison with previous experimental studies[31,52] and computational results.[53]

## V. Conclusions

For the first time, an unsteady PSP system capable of measuring sub-psi surface pressure differentials has been successfully implemented at full scale in the TDT. Due to the inoperable condition of the facility main drive during the testing window, an unsteady flow system was utilized to produce spatiotemporal pressure fluctuations on the surface of a generic launch vehicle model. Signal intensity data were collected at camera framerates of 5 and 10 kHz for various model attitudes, and were processed using the NASA Pleiades supercomputer to provide measurements of pressure. Pressure time histories obtained using uPSP were compared with measurements from unsteady Kulite sensors and showed agreement for both the phase and amplitude of oscillations. Spectral analysis indicated that both systems are capable of measuring the fundamental frequency (as well as the second and third harmonics) of the passive oscillator used to provide the unsteady flow driving the surface pressure fluctuations. Results were post-processed using DMD to determine the dominant spatial coherent structures (along with their associated frequencies and growth rates), allowing for a denoised reconstruction of the uPSP measurements considering only the 25 leading modes. Future work will further explore the influence of the number of modes considered in the DMD analysis and refine the mode cutoff value. Since the studies considered in this report were conducted exclusively in air, another important factor to be considered in future testing at the TDT is the ability to measure surface pressure fluctuations in a low $O_2$ environment and determine the $O_2$ concentration required for uPSP measurements made when the wind tunnel facility is operating using R-134a as the test medium.

## Acknowledgments

This work would never have been possible without valuable contributions from dozens of people. The authors wish to extend their sincerest thanks to test engineers Sky Seliquini, Mark Wason, and Cody Pierce; TDT staff John Ferguson, Matt Woolever, Mike Charnock, Hugo Perez, Andrew Yach, Mark Bailey, Juanita Ford, John Meador, Mike Normand, and Pat Weymouth; members of the Aeroelasticity Branch Jen Heeg, Bill Stevens, Dave Piatak, Patrick Heaney, Francesco Soranna, Martin Sekula, Ian Giles, Oleg Goushcha, Lee Mears, and Mike Ramey; Ames researchers Nettie Roozeboom and Marc Shaw-Lecerf for their collaboration regarding uPSP processing; and members of the Advanced Measurements and Data Systems Branch Brett Bathel and Paul Danehy for their assistance with the design and purchase of the environmental enclosures. Resources supporting this work were provided by the NASA High-End Computing (HEC) Program through the NASA Advanced Supercomputing (NAS) Division at NASA Ames Research Center. This work was

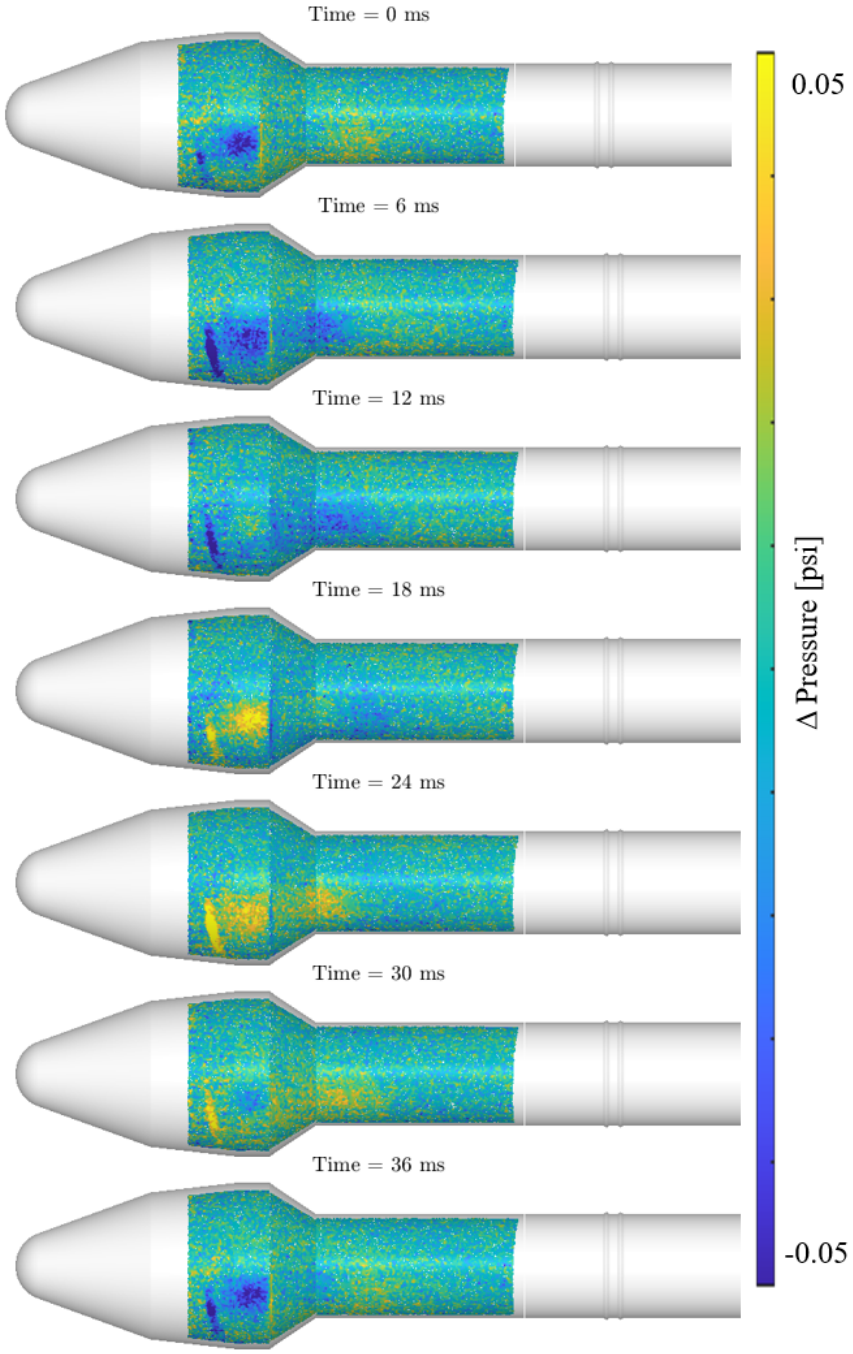


**Figure 10. DMD reconstruction of uPSP results mapped to the grid. Time-series of images showing the dynamics of the leading 25 modes for the measured surface pressure.**

funded by the NASA Aeronautics Research Mission Directorate Transformational Tools and Technologies project.

## References

[1]Alter, S. J., Brauckmann, G. J., Kleb, B., Glass, C. E., Streett, C. L., and Schuster, D. M., "Time-Accurate Unsteady Pressure Loads Simulated for the Space Launch System at Wind Tunnel Conditions," 33rd AIAA Applied Aerodynamics Conference, AIAA Aviation Forum, 2015.

[2]Soranna, F., Heaney, P. S., Sekula, M. K., Piatak, D. J., Ramey, J. M., Roozeboom, N., Murakami, D. D., Baerny, J. K., Li, J., Stremel, P. M., and Powell, J. M., "Analysis of Buffet Forcing Functions Estimated from Unsteady Pressure Sensitive Paint," AIAA Aviation Forum, 2020.

[3]Heaney, P. S., Soranna, F., Sekula, M. K., Piatak, D. J., and Ramey, J. M., "Analysis of Transonic Unsteady Aerodynamic Environments using Unsteady Pressure Sensitive Paint for the Space Launch System Block 1 Cargo Launch Vehicle," AIAA SciTech Forum, 2021.

[4]Schuster, D. M., Panda, J., Ross, J. C., Roozeboom, N. H., Burnside, N. J., Ngo, C. L., Kumagai, H., Sellers, M., Powell, J. M., Sekula, M. K., and Piatak, D. J., "Investigation of Unsteady Pressure-Sensitive Paint (uPSP) and a Dynamic Loads Balance to Predict Launch Vehicle Buffet Environments," NASA TP-2016-219352, Nov. 2016.

[5]Sekula, M. K., Piatak, D. J., Rausch, R. D., Ross, J. C., and Sellers, M. E., "Assessment of Buffet Forcing Function Development Process Using Unsteady Pressure Sensitive Paint," AIAA Aviation 2019 Forum, American Institute of Aeronautics and Astronautics, 2019.

[6]Sekula, M. K., Piatak, D. J., and Rausch, R., "Effect of Surface Pressure Integration Methodology on Launch Vehicle Buffet Forcing Functions," 54th AIAA Aerospace Sciences Meeting, 2016.

[7]Sekula, M. K., Piatak, D. J., Rausch, R., Florance, J. R., and Ramey, J., "Initial Assessment of Space Launch System Transonic Unsteady Pressure Environment," 53rd AIAA Aerospace Sciences Meeting, AIAA SciTech Forum, 2015.

[8]Morris, M.J., Benne, M.E., Crites, R.C., and Donovan, J.F., "Aerodynamic Measurements Based on Photoluminescence," 31st Aerospace Sciences Meeting and Exhibit, AIAA Paper 93-0175, 1993.

[9]McLachlan, B., and Bell, J., "Pressure-Sensitive Paint in Aerodynamic Testing," Experimental Thermal and Fluid Science, Vol. 10, No. 4, 1995, pp. 470-485.

[10]Liu. T., Campbell, B., Burns, S., and Sullivan, J., "Temperature- and Pressure-Sensitive Luminescent Paints in Aerodynamics," Applied Mechanics Reviews, Vol. 50, No. 4, 1997, pp. 227-246.

[11]Liu, T., and Sullivan, J., Pressure and Temperature Sensitive Paints (Experimental Fluid Dynamics), Springer-Verlag, Berlin, 2005, pp. 1-36.

[12]Sellers, M. E. "Advances in AEDC's Lifetime Pressure-Sensitive Paint Program." U.S. Air Force T&E Days, Nashville, TN, AIAA Paper 2005-7638, December 2005.

[13]Sellers, M. E. "AEDC's Portable Pressure-Sensitive Paint Data Acquisition System." U.S. Air Force T&E Days, Destin, FL, AIAA Paper 2007-1606, February 2007.

[14]Sellers, M. E. "Validation of Integrated Panel Loads on a Fighter Aircraft Model Using Pressure-Sensitive Paint at AEDC." AEDC-TMR-08-T2, January 2008.

[15]Sellers, M. E. "Pressure-Sensitive Paint Data on the Facility Aerodynamics Validation and Research (FAVOR) Model at AEDC." AEDC-TR-09-F-34, December 2009.

[16]Sellers, M. E. "Demonstration of a Temperature-Compensated Pressure Sensitive Paint on the Orion Launch Abort Vehicle." 29th AIAA Applied Aerodynamics Conference, Honolulu, HI, AIAA Paper 2011-3166, June 2011.

[17]Gregory, J.W., Asai, Sakaue, H., Liu, T., and Sullivan, J.P., "Fast Pressure-Sensitive Paint for Flow and Acoustic Diagnostics," Annual Review of Fluid Mechanics, Vol. 46, 2014, pp. 303-330.

[18]Liu, T., Torgerson, S., Sullivan, J., Johnston, R., and Fleeter, S., "Rotor Blade Pressure Measurement in a High Speed Axial compressor Using Pressure and Temperature Sensitive Paints," 35th Aerospace Sciences Meeting and Exhibit, AIAA Paper 1997-0162, 1997.

[19]Torgerson, S, Liu, T., and Sullivan, J., "Rotor Blade Pressure Measurement in a Rotating Machinery Using Pressure and Temperature Sensitive Paints," AGARD-CP-598-Advanced Non-Intrusive Instrumentation for Propulsion Engines, pp. 19-1-19-9, 1998.

[20]Bencic, T.J., "Rotating pressure and temperature Measurements on Scale-Model Fans Using Luminescent Paints," 34th AIAA/ASME/SAE/ASEE Joint Propulsion Conference and Exhibit, AIAA Paper 1998-3452, 1998.

[21]Navarra, K., Goss, L., Jordan, J., Rabe, D., Gord, J., Car, D., "Optical Measurements of Surface Pressure and Temperature in Turbomachinery," AGARD-CP-598-Advanced Non-Intrusive Instrumentation for Propulsion Engines, pp. 18-1-18-13, 1998.

[22]Gregory J.W., "Porous Pressure-Sensitive Paint for Measurement of Unsteady Pressures in Turbomachinery," 42nd Aerospace Sciences Meeting, AIAA, Reno, NV, 2004, Paper 2004-0294.

[23]Suryanarayanan, A., Mhetras, S.P., Schobeiri, M.T., and Han, J-C., "Film-Cooling Effectiveness on a Rotating Blade Platform," ASME Turbo Expo 2006: Power for Land, Sea, and Air, Volume 3: Heat Transfer, Parts A and B, American Society of Mechanical Engineers, 2006, pp. 37-47.

[24]Ahn, J., Schobeiri, M.T., Han, J-C., and Moon, H-K., "Film Cooling Effectiveness on the Leading Edge Region of a Rotating Turbine Blade with Two Rows of Film Cooling Holes Using Pressure Sensitive Paint," Journal of Turbomachinery, Vol. 128, No. 9, 2006, pp. 879-888.

[25]Suryanarayanan, A., Ozturk, B., Schobeiri, M.T., and Han, J-C., "Film-Cooling Effectiveness on a Rotating Turbine Platform Using Pressure Sensitive Paint Techniuqe," Journal of Turbomachinery, Vol. 132, No. 1, 2010, pp. 041001-041001-13.

[26]Wong, O.D., Watkins, A.N., and Ingram, J.L., "Pressure Sensitive Paint Measurements on 15% Scale Rotor Blades in Hover," 35th AIAA Fluid Dynamics Conference, Toronto, Ontario Canada, AIAA Paper 2005-5008, 2005.

[27]Watkins, A.N., Leighty, B.D., Lipford, W.E., Wong, O.D., Oglesby, D.M., and Ingram, J.L., "Development of a Pressure Sensitive Paint System for Measuring Global Surface Pressures on Rotorcraft Blades," 22nd International Congress on Instrumentation in Aerospace Simulation Facilities, Institute of Electrical and Electronics Engineers, Piscataway, NJ, 2007.

[28]Wong, O.D., Watkins, A.N., Goodman, K.Z., Crafton, J., Forlines, A., Goss, L., Gregory, J.W., and Juliano, T.J., "Blade Tip Pressure Measurements Using Pressure Sensitive Paint," Proceedings of the AHS International 68th Annual Forum, Fort Worth, TX, May 103, 2012.

[29]Watkins, A.N., Leighty, B.D., Lipford, W.E., Wong, O.D., Goodman, K.Z., Crafton, J., Forlines, A., Goss, L.P., Gregory, J.W., and Juliano, T.J., "Development of a Pressure Sensitive Paint System for Measuring Global Surface Pressures on Rotorcraft Blades in Simulated Forward Flight," 28th Aerodynamic Measurement Technology, Ground Testing, and Flight Testing Conference, New Orleans, LA, AIAA Paper 2012-2756, 2012.

[30]Kavandi, J., Callis, J., Gouterman, M., Khalil, G., Wright, D., Green, E., Burns, D., and McLachlan, B., "Luminescent Barometry in Wind Tunnels," Review of Scientific Instrumentation, Vol. 61, No. 11, 1990, pp. 3340-3347.

[31]Sellers, M. E., Nelson, M. A., Roozeboom, N. H., and Burnside, N. H., "Evaluation of Unsteady Pressure Sensitive Paint Measurement Technique for Space Launch Vehicle Buffet Determination," 55th AIAA Aerospace Sciences Meeting, Grapevine, TX, AIAA Paper 2017-1402, 2017.

[32]Roozeboom, N., Powell, J., Baerny, J., Murakami, D., Ngo, C., Garbeff, T., Ross, J., Flach, R., "Development of Unsteady Pressure-Sensitive Paint Application on NASA Space Launch System", AIAA Aviation Forum, Dallas, TX, AIAA 2019-3502, June 2019.

[33]Roozeboom, N., Baerny, J. K., Murakami, D. D., Ngo, C., and Powell, J. M., "Recent Developments in NASA's Unsteady Pressure-Sensitive Paint Capability," AIAA Scitech Forum, Orlando, FL, AIAA Paper 2020-0516, 2020.

[34]Corliss, J.M., and Cole, S.R., "Heavy Gas Conversion of the NASA Langley Transonic Dynamics Tunnel," 20th AIAA Advanced Measurement and Ground Testing Technology Conference, June 15 – 18, 1998, Albuquerque, NM (AIAA Paper 98-2710).

[35]Cole, S.R., Noll, T.E., and Perry, B., "Transonic Dynamics Tunnel Aeroelastic Testing in Support of Aircraft Development," Journal of Aircraft, Vol. 40, No. 5, 2003.

[36]Wieseman, C.D., and Sleeper, R.K., "Measurements of Flow Turbulence in the NASA Langley Transonic Dynamics Tunnel," NASA TM 2005-213529, February 2005.

[37]Florance, J.R., and Rivera, J.A., "Sidewall Mach Number Distributions for the NASA Langley Transonic Dynamics Tunnel," NASA TM-2001-211019.

[38]Yeager, W.T., Wilbur, M.L., Rivera, J.A., Mirick, P., "Flow Angularity Measurements in the NASA-Langley Transonic Dynamics Tunnel," NASA TM-2005-213946, Dec. 2005.

[39]Wieseman, C.D., and Bennett, R.M., "Wall Boundary Layer Measurements for the NASA Langley Transonic Dynamics Tunnel," NASA TM-2007-214867, April 2007.

[40]Piatak, D.J., "Survey of Primary Flow Measurement Parameters at the NASA Langley Transonic Dynamics Tunnel," NASA TM-2003-212413, June 2003.

[41]Ivanco, T.G., "Unique Testing Capabilities of the NASA Langley Transonic Dynamics Tunnel, an Exercise in Aeroelastic Scaling," AIAA Ground Testing Conference, San Diego, CA, AIAA 2013-2625, pp. 1–23, 2013.

[42]Reed, W. H., "Aeroelasticity Matters: Some Reflections on Two Decades of Testing in the NASA Langley Transonic Dynamics Tunnel," NASA TM83210, Sept. 1981.

[43]Cole, S. R., Keller, D. F., and Piatak, D. J., "Contributions of the Transonic Dynamics Tunnel to Launch Vehicle and Spacecraft Development," AIAA Dynamics Specialists Conference, Atlanta, GA, AIAA Paper 2000-1772, April 2000.

[44]Perry, B., III, Noll, T. E., and Scott, R. C., "Contributions of the Transonic Dynamics Tunnel to the Testing of Active Control of Aeroelastic Response," AIAA Dynamics Specialists Conference, Atlanta, GA, AIAA Paper 2000-1769, April 2000.

[45]Schuster, D. M., Edwards, J. W., and Bennett, R. M., "An Overview of Unsteady Pressure Measurements in the Transonic Dynamics Tunnel," AIAA Dynamics Specialists Conference, Atlanta, GA, AIAA Paper 2000-1770, April 2000.

[46]Rivera, J. A., and Florance, J. R., "Contributions of Langley Transonic Dynamics Tunnel Testing to Airplane Flutter Clearance," AIAA Dynamics Specialists Conference, Atlanta, GA, AIAA Paper 2000-1768, April 2000.

[47]Cole, S. R., and Garcia, J. L., "Past, Present, and Future Capabilities of the Transonic Dynamics Tunnel from and Aeroelasticity Perspective," AIAA Dynamics Specialists Conference, Atlanta, GA, AIAA Paper 2000-1767, April 2000.

[48]Piatak, D. J., and Cleckner, C. S., "Oscillating Turntable for the Measurement of Unsteady Aerodynamic Phenomena," Journal of Aircraft, Vol. 40, No. 1, 2003, pp. 181–188.

[49]M. Koklu, "Fluidic oscillator having decoupled frequency and amplitude control." U.S. Patent 9,339,825, issued May 17, 2016.

[50]Charles F. Coe and James B. Nute. "Steady and fluctuating pressures at transonic speeds on hammerhead launch vehicles," Technical Report X-778, NASA Ames Research Center, Moffett Field, California, December 1962.

[51]Garbeff, T. J., Panda, J., Ross, J. C., and Smith, N. T., "Experimental Visualizations of a Generic Launch Vehicle Flow Field: Time-Resolved Shadowgraph and Infrared Imaging," 55th AIAA Aerospace Sciences Meeting, AIAA Paper 2017-1403, 2017.

[52]Panda, J., Roozeboom, N. H., and Ross, J. C., "Wavenumber-Frequency Spectra on a Launch Vehicle Model Measured via Unsteady Pressure-Sensitive Paint," AIAA Journal, 2019, pp. 1–17.

[53]Scott M. Murman, Laslo T. Diosady, Patrick J. Blonigan, "Comparison of transonic buffet simulations with unsteady PSP measurements for a hammerhead payload fairing," 55th AIAA Aerospace Sciences Meeting: AIAA SciTech Forum, Grapevine, TX, AIAA Paper 2017-1404, January 2017.

[54]Ivanco, T. G., "Software Design and Interface Design Description (ABDAS Architecture)." Technical report, NASA Langley Research Center, Hampton, Virginia, February 2020.

[55]Ivanco, T. G., Piatak, D. J., Sekula, M. K., Simmons, S. A., Babel, W. C., Collins, J. G., Ramey, J. M., Heald, D. M., "A New High Channel-Count, High Scan-Rate, Data Acquisition System for the NASA Langley Transonic Dynamics Tunnel," Proceedings of the 54th AIAA Aerospace Sciences Meeting, AIAA 2016-1149.

[56]R. Biswas, et al., "Pleiades: NASA's First Petascale Supercomputer," Contemporary High Performance Computing: From Petascale toward Exascale, edited by J. Vetter, Chapman and Hall/CRC, 2013, pp. 309–338.

[57]Jin, H., D. Jespersen, P. Mehrotra, R. Biswas, L. Huang, and B. Chapman (2011), High performance computing using MPI and OpenMP on multi-core parallel systems, Parallel Comput., 37(9), 562–575.

[58]Powell, J. M., Murman, S. M., Ngo, C., Roozeboom, N., Murakami, D. D., Baerny, J. K., and Lie, J., "Development of Unsteady-PSP Data Processing and Analysis Tools for the NASA Ames Unitary 11ft Wind Tunnel," AIAA SciTech Forum, Orlando, FL, AIAA Paper 2020-0292, January 2020.

[59]Schlichting, H., *Boundary-Layer Theory*, McGraw-Hill, New York, 1979.

[60]Schmid, P. J., "Dynamic mode decomposition of numerical and experimental data." Journal of Fluid Mechanics 656.1 (2010): 5–28.

[61]Li, J., Lash, L., Roozeboom, N., Garbeff, T., Henze, C., Murakami, D., Smith, N., Baerny, J., Hand, L., Shaw-Lecerf, M., Stremel, P., and Tang, L., "Dynamic Mode Decomposition of Unsteady Pressure-Sensitive Paint Measurements for the NASA Unitary Plan Wind Tunnel Tests," AIAA Paper 2022-0141, AIAA SciTech Forum, San Diego, CA, January 2022.

[62]Ali, M.Y., Pandey, A., and Gregory, J.W., "Dynamic Mode Decomposition of Fast Pressure Sensitive Paint Data," Sensors, Vol. 16, No. 6, 2016, 862.

[63]Gößling, J., Ahlefeldt, T., and Hilfer, M., "Experimental Validation of Unsteady Pressure-Sensitive Paint for Acoustic Applications," Experimental Thermal and Fluid Science, V. 112, 2020, 109915.

[64]Cattell, Raymond B. (1966). "The Scree Test For The Number Of Factors". Multivariate Behavioral Research. 1 (2): 245–276.

[65]Tu, J. H., Rowley, C. W., Luchtenburg, D. M., "On dynamic mode decomposition: theory and applications," Journal of Computational Dynamics, 1 (2), 391–421 (2014).